



## Article

# Optical Properties of KTP Crystals and Their Potential for Terahertz Generation

Alexander Mamrashev <sup>1,\*</sup> , Nazar Nikolaev <sup>1</sup> , Valery Antsygin <sup>1</sup>, Yury Andreev <sup>2,3</sup>, Grigory Lanskii <sup>2,3</sup> and Arkady Meshalkin <sup>4</sup>

<sup>1</sup> Institute of Automation & Electrometry, SB RAS, 1, Ac. Koptuyug Ave., Novosibirsk 630090, Russia; nazar@iae.nsk.su (N.N.); antsygin@iae.nsk.su (V.A.)

<sup>2</sup> Institute of Monitoring of Climatic and Ecological Systems, SB RAS, 10/3, Akademicheskii Ave., Tomsk 634055, Russia; yuandreev@yandex.ru (Y.A.); lansky@yandex.ru (G.L.)

<sup>3</sup> Siberian Physical Technical Institute of Tomsk State University, 1 Novosobornaya Sq., Tomsk 634050, Russia

<sup>4</sup> Institute of Thermophysics, SB RAS, 1, Ac. Lavrent'ev Ave., Novosibirsk 630090, Russia; kaplun@itp.nsc.ru

\* Correspondence: mamrashev@iae.nsk.su; Tel.: +7-383-330-8378

Received: 30 June 2018; Accepted: 28 July 2018; Published: 31 July 2018



**Abstract:** High nonlinearity, wide transparency range and optical quality allowed potassium titanyl phosphate (KTiOPO<sub>4</sub>, KTP) crystals to be used in a wide range of nonlinear applications. The success of KTP usage in the visible and infrared (IR) ranges drives interest in applying it at longer wavelengths, that is, in the terahertz (THz) range. We use THz optical properties of KTP crystals measured by terahertz time-domain spectrometer (THz-TDS) and refractive index approximated in the form of Sellmeier equations to investigate KTP application possibilities for IR-to-THz and THz-to-THz wave conversion. As a result, phase matching for  $s - f \rightarrow f$  and  $s - f \rightarrow s$  types of difference frequency generation (DFG) of Ti:Sapphire laser (at the wavelengths of 0.65, 0.8 and 1.1  $\mu\text{m}$ ) is found possible, as well as second harmonic generation (SHG) of THz waves by  $f + s \rightarrow f$  type of interaction in the *XZ* principle plane of the crystal. Terahertz wave generation by phase-matched parametric processes in KTP demonstrates evident advantages in comparison with that of widely used MgO-doped LiNbO<sub>3</sub> crystals.

**Keywords:** KTP; nonlinear crystal; frequency conversion; SHG; DFG; THz radiation; THz wave

## 1. Introduction

Potassium titanyl phosphate (KTiOPO<sub>4</sub>, KTP) is one of the most widely used nonlinear optical crystals [1]. KTP belongs to the *mm2* point group symmetry and its dielectric and crystallographic axes are assigned as *X, Y, Z*  $\rightarrow$  *a, b, c*. Its structure consists of chains of connected rigid PO<sub>4</sub> tetrahedra and TiO<sub>6</sub> octahedra with alternating long and short Ti–O bonds that are responsible for its nonlinear properties [2]. KTP advantages are high nonlinear coefficients:  $d_{15} = 1.9$  pm/V,  $d_{24} = 4.2$  pm/V,  $d_{31} = 2.2$  pm/V,  $d_{32} = 2.7$  pm/V and  $d_{33} = 17.4$  pm/V, wide ranges of angles and temperatures for the phase matching, low absorption in the range of 0.35  $\mu\text{m}$  to 4.5  $\mu\text{m}$ , excellent mechanical stability and optical quality. One of the few KTP disadvantages is its susceptibility to photochromic damage, that is, grey-tracking, that causes slow deterioration of light conversion efficiency.

The abovementioned properties of KTP determine its wide range of nonlinear applications such as sum [3] and difference [4,5] frequency generation (SFG and DFG), second harmonic generation (SHG) [6], optical parametric oscillation/generation (OPO/OPG) and amplification (OPA) [7–9]. Parametric generation based on stimulated polariton scattering in KTP shows superior performance in terms of gain and laser damage resistance in comparison to lithium niobate and lithium tantalate [10,11]. Other KTP applications include modulators for the near- and the mid-IR ranges [12–14].

The success of KTP nonlinear applications in the visible and IR ranges drives interest in studying its terahertz dielectric and optical (THz) properties to substitute the widely used pure and MgO-doped lithium niobate crystals (LiNbO<sub>3</sub>, LN) in this range [15]. Previously, infrared reflectivity spectrum of KTP was studied up to the wavenumber of 4000 cm<sup>−1</sup> (120 THz) at the temperatures of 7 K, 80 K and 293 K [16]. Later, the results were supplemented by Raman spectroscopy measurements at the wavenumbers below 4000 cm<sup>−1</sup> [17]. Recently, THz refractive index and absorption coefficient were directly measured using growingly accessible THz time-domain spectrometers (THz-TDS) [18–21]. The most comprehensive study of its THz optical properties for the waves polarized parallel to all three optical axes of the KTP crystals was carried out in [20]. The refractive index components at room temperature were approximated in the form of Sellmeier equations [21].

In this paper, we report terahertz optical properties of KTP crystals at the room temperature of 293 K (RT) and at the liquid nitrogen temperature of 81 K and calculate phase-matching conditions for nonlinear frequency conversion into and within the THz range.

## 2. Materials and Methods

KTP single-crystal ingots were grown using the Czochralski method from a Pt crucible of 100 mm in diameter. The crucible closed with Pt cover with about 1 kg of charge was disposed in the resistivity oven. After heating, the melt was homogenized and cooled down to liquidus temperature. The crystals were grown using single-domain seed in the direction of X-axis. During the growth period of 45–55 days, the melt was cooled down by 70–120 °C. The cooling rate of the crystal was 0.1–4 °C/day while its rotation speed varied from 30 to 40 rpm. In parallel, the pulling speed changed from 0 to 1.2 mm/day. By selecting optimal growth conditions high-quality single-crystal ingots having a weight of 260 g and dimensions of  $X \times Y \times Z = 40 \times 60 \times 70$  mm<sup>3</sup> were grown.

At first, a large plate with dimensions of  $X \times Y \times Z = 11 \times 28 \times 58$  mm<sup>3</sup> was manufactured to evaluate the quality of the grown crystal and measure its transmission spectrum in the main transparency window. Then three pairs samples with different thickness with dimensions of  $10 \times 10 \times (0.28, 0.35 \text{ and } 1.08)$  mm<sup>3</sup> were cut orthogonal to the optical axes  $X$  (KTP<sub>x</sub>) and  $Z$  (KTP<sub>z</sub>) (Figure 1). Sides of the KTP<sub>x</sub> sample were parallel to the  $Y$  and  $Z$  axes and sides of the KTP<sub>z</sub> sample were parallel to the  $X$  and  $Y$  axes. So, every pair of samples allowed us to measure all three ( $x$ ,  $y$  and  $z$ ) components of the absorption coefficient and refractive index for waves polarized parallel to the  $X$ ,  $Y$  and  $Z$  axes, respectively and select the best-thickness crystals for the study.

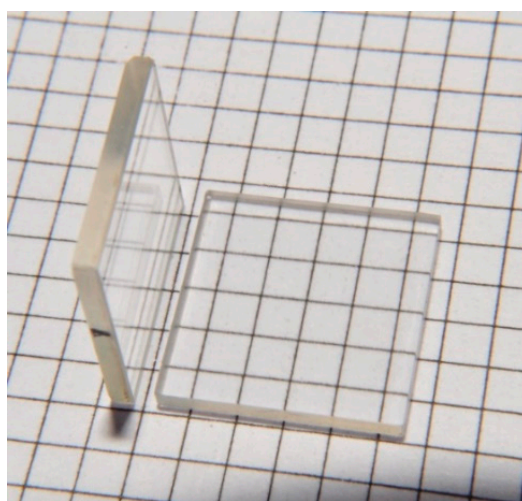


**Figure 1.** A pair of prepared KTP crystal samples cut orthogonal to the  $X$  and  $Z$  axes.

Transmission spectra in the transparency window were measured by UV-2101/3101 spectrophotometer (Shimadzu, Kyoto, Japan). Terahertz optical properties were studied using

a THz-TDS (IA&E SB RAS, Novosibirsk, Russia) with a cryostat described elsewhere [20] at the temperatures of 293 K and 81 K.

### 3. Results

The resistivity of a grown KTP crystal is one of indicators of its quality. Higher values of resistivity make the crystals applicable for manufacturing electro-optic devices: amplitude and phase modulators [12]. Figure 2a depicts crystal resistivity which stays larger than  $10^{11} \Omega \text{ cm}$  for the applied electric field up to 20 kV/cm proving high quality and easy polarizability of the samples for creating periodical structures. Visible and IR range transmission spectrum of thick KTP plate for the wave propagating along X axis and polarized parallel to Z axis is presented in Figure 2a. The quality of the grown crystals is additionally supported by the lack of a wide absorption band around 2800 nm that is attributed to O–H bonds. The measured transmission corresponds to absorption coefficients below  $10^{-3} \text{ cm}^{-1}$ . Thus, KTP crystals can be pumped in the range of 0.375–4.2  $\mu\text{m}$  by visible and IR radiation including chemical lasers. The absence of two-photon absorption while pumping by widely used all-solid-state lasers such as Ti:Sapphire (0.8–1.1  $\mu\text{m}$ ), Nd:YAG (1.064  $\mu\text{m}$ ), holmium (2.01  $\mu\text{m}$ ), erbium (2.94  $\mu\text{m}$ ) and  $\text{Fe}^{2+}:\text{ZnSe}$  (4.1  $\mu\text{m}$ ) is attractive for applied systems.

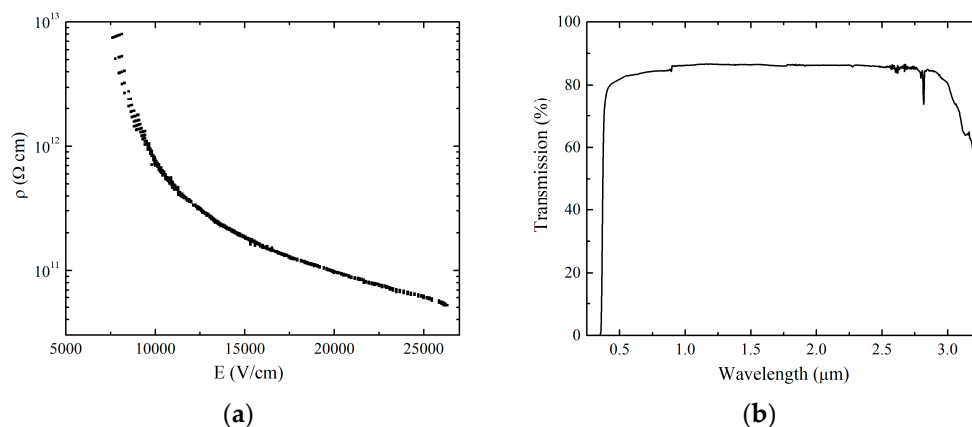


**Figure 2.** (a) A typical dependence of resistivity on the applied electric field of the grown KTP ingot; (b) Transmission spectra of thick KTP plate for radiation polarized parallel to Z axis in the visible and IR ranges.

Absorption of the KTP crystal recorded by THz-TDS decreases at higher wavelengths (Figure 3). This behaviour arises from the presence of several phonon modes below 200  $\mu\text{m}$ . X and Y axes demonstrate the lowest absorption ( $<5 \text{ cm}^{-1}$  for wavelengths  $>360 \mu\text{m}$ ) especially after cooling down to 81 K ( $<1 \text{ cm}^{-1}$  for wavelengths  $>250 \mu\text{m}$ ). The measured absorption coefficient of KTP crystal is significantly lower compared to 0.7% MgO-doped stoichiometric lithium niobate which is preferable for terahertz wave generation (see Figure 3a for comparison) [22,23]. The wavelengths above 500  $\mu\text{m}$  are also free from strong water vapour absorption lines and are of interest for gas analysis with THz lidar.

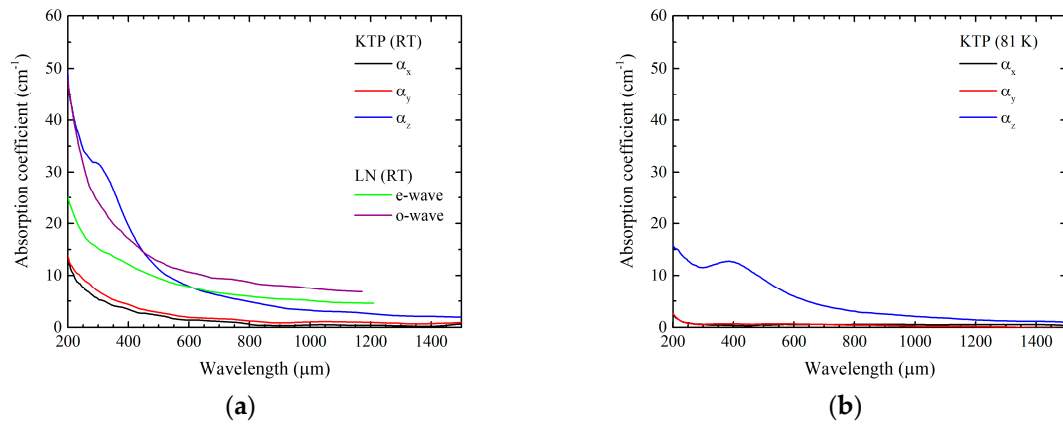


**Figure 3.** Measured absorption coefficient of KTP compared to 0.7% MgO-doped stoichiometric lithium niobate (LN, adapted from [23]) at: (a) Room temperature; (b) Liquid nitrogen temperature.

Refractive index components for the long-wavelength terahertz range measured by TH-TDS at the room and liquid nitrogen temperatures are shown in Figure 4a,b, respectively.

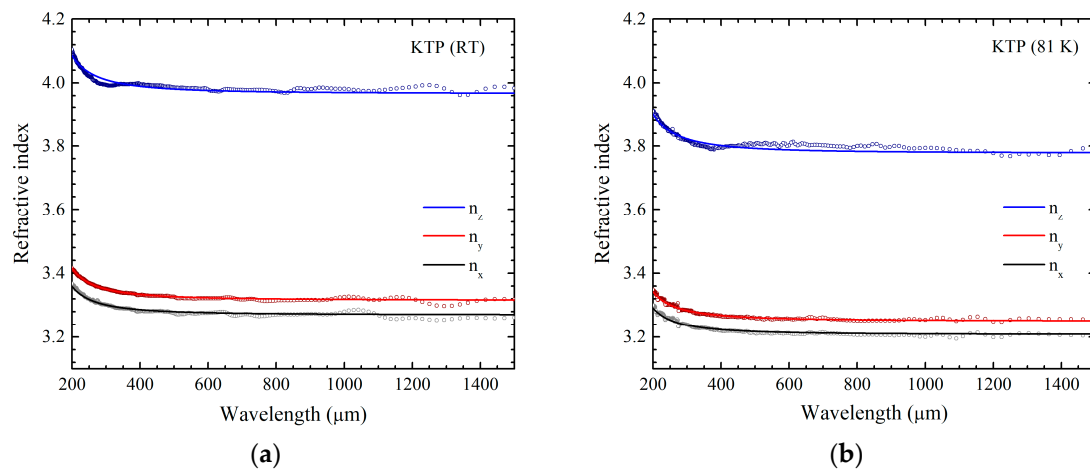


**Figure 4.** Measured (circles) and approximated (solid lines) dispersion of refractive index components of KTP at: (a) Room temperature; (b) Liquid nitrogen temperature.

Recorded dispersions were approximated in the form of Sellmeier equations by the best-fit method within the spectral range of 142  $\mu\text{m}$  to 1500  $\mu\text{m}$  at the room temperature [21]:

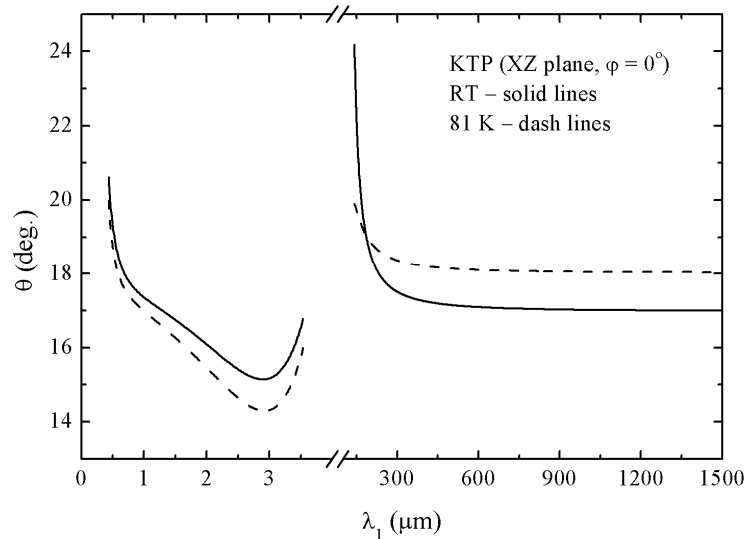
$$\begin{aligned} n_x^2 &= 9.54967 + \frac{1.14398\lambda^2}{\lambda^2 - 13637}, \\ n_y^2 &= 9.72515 + \frac{1.26864\lambda^2}{\lambda^2 - 13889}, \\ n_z^2 &= 13.4416 + \frac{2.29045\lambda^2}{\lambda^2 - 11799}. \end{aligned} \quad (1)$$

Corresponding Sellmeier equations for 81 K could be written as follows:

$$\begin{aligned} n_x^2 &= 9.07963 + \frac{1.20539\lambda^2}{\lambda^2 - 12497}, \\ n_y^2 &= 9.20704 + \frac{1.36025\lambda^2}{\lambda^2 - 12264}, \\ n_z^2 &= 11.8979 + \frac{2.36823\lambda^2}{\lambda^2 - 11336}. \end{aligned} \quad (2)$$

Approximation curves calculated using sets of Equations (1) and (2) are also depicted in Figure 4. It should be emphasized that the KTP refractive index is much smaller than that of LiNbO<sub>3</sub> crystals (~5.2) [22] and collinear velocity-matching appears to be possible in contrast to LN crystal.

By using known dispersion equations for the refractive index for the main transparency window and its temperature dependence [1] and Equations (1) and (2), the dependence of  $V_z$  angle versus wavelength is calculated for the entire transparency range of KTP (Figure 5).



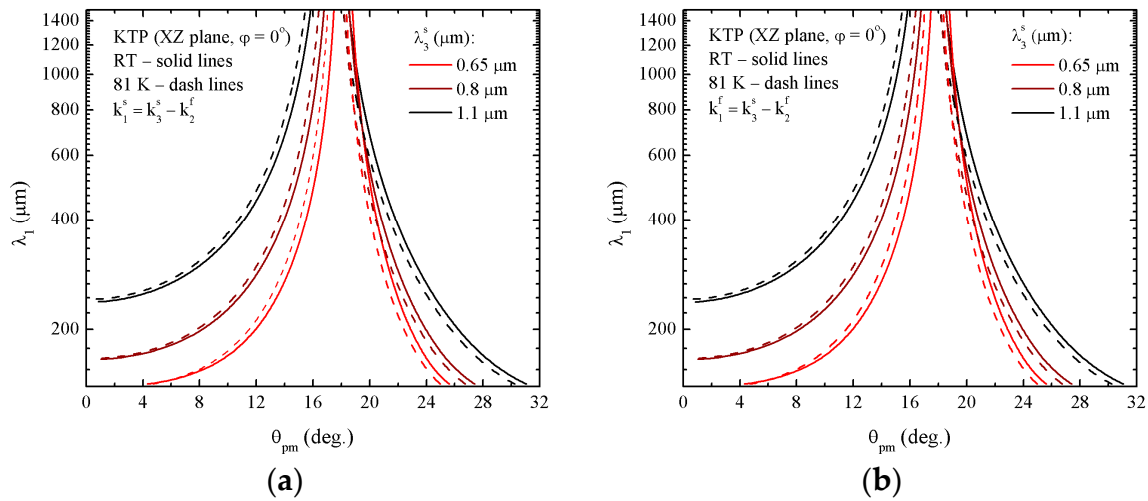
**Figure 5.** Spectral dependence of the  $V_z$  angle in the principle  $XZ$  plane at RT and 81 K.

Figure 5 shows that  $V_z$  angle is weakly dependent on the crystal temperature, that is, phase-matching should be also insensitive to the temperature variations in contrast to LiNbO<sub>3</sub> [15]. It is interesting to note that  $V_z$  position in the long wavelength region of the THz range is not dependent on the wavelength, that is, effective nonlinearity is not dependent on the pump wavelength for frequency conversion processes within it.

Phase matching for difference frequency generation into the THz range under visible and near-IR pump is found possible only in the principle  $XZ$  plane (at  $\theta > V_z$  and  $\theta < V_z$ ) at RT and 81 K by  $s - f \rightarrow f$  and  $s - f \rightarrow s$  types of interactions. Here,  $s$  and  $f$  symbols denote slow and fast interacting waves, respectively. For example, phase-matching curves for frequency conversion of tunable (0.65–1.1  $\mu\text{m}$ ) Ti:Sapphire laser are presented in Figure 6.

It is seen in Figure 6 that type I and type II interactions have very close phase-matching conditions. For interactions in the  $XZ$  plane, when Kleinman symmetry conditions are not valid, effective nonlinear coefficient is  $d_{s-f \rightarrow f} = d_{32} \cdot \sin\theta$  for  $\theta < V_z$  and  $d_{s-f \rightarrow s} = d_{24} \cdot \sin\theta$  for  $\theta > V_z$  [1]. At 1.064  $\mu\text{m}$   $d_{24} \approx d_{32} = 3.7 \text{ pm/V}$ . So, DFG at larger angles is preferable for both processes due to higher nonlinear coefficient and smaller absorption. Group velocity matching at  $\theta > V_z$  is better for the shortest pump wavelength. Thus, ultrashort pulse conversion can be more efficient, for example, under the pump of THL-100 hybrid laser system built in the Institute of High Current Electronics, Siberian Branch of Russian

Academy of Sciences:  $\lambda = 475$  nm (wavelength),  $\tau = 50$  fs (pulse duration),  $d = 25$  cm (pulse aperture),  $P = 14$  TW (pulse power) and  $E = 1$  J (pulse energy) [24].



**Figure 6.** Phase-matching curves for DFG (a)  $s - f \rightarrow f$  and (b)  $s - f \rightarrow s$  types of Ti:Sapphire laser (at 0.65, 0.8 and 1.1  $\mu\text{m}$ ): optical rectification or mixing of two close wavelength lasers in the  $XZ$  principle plane of KTP crystal at RT (solid lines) and 81 K (dashed lines) versus  $\theta$  angle.

By using relations (1) and (2), phase matching for collinear second harmonic generation of THz waves is also found possible by type I ( $s + s \rightarrow f$ ) and type II ( $f + s \rightarrow f$ ) of three-wave interactions in the  $XZ$  plane. Figure 7 plots the phase-matching curves for type II SHG. Phase-matching conditions for type I and type II SHG of longer THz waves are found close to each other, that is, their efficiencies also should be close. Cooling down KTP crystal to 81 K results in a small ( $1^\circ$ ) increase of  $V_z$  angle (Figure 5) but it provides with efficient control of group velocity matching conditions.

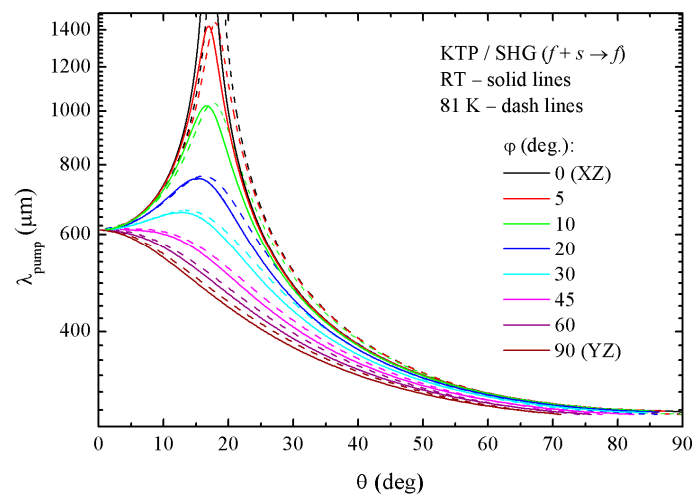


**Figure 7.** Phase-matching curves for SHG of THz waves by  $f + s \rightarrow f$  type of interaction in the  $XZ$  principle plane of KTP versus  $\theta$  and  $\varphi$  angles that is identified in the figure inset.

#### 4. Discussion

It can be proposed that minimal absorption coefficient of KTP crystal is determined by the residual domain structure that can be decreased by application of higher voltage and further optimization of the growth process. Further cooling below 81 K can narrow the phonon lines and decrease their



wavelength extending the THz transparency range toward shorter wavelengths. Furthermore, cooling can increase the damage threshold leading to improved frequency conversion efficiency that is a subject of future study. THz wave energy can be seriously scaled up by using large aperture KTP samples pumped by ultrashort pulse terawatt (TW) laser systems that should be studied experimentally.

Finally, low absorption at visible-IR pump wavelengths and long THz wavelengths ( $\geq 500 \mu\text{m}$  at RT and  $125 \mu\text{m}$  at 81 K) together with the exceptional set of known physical properties render KTP crystal amongst the most prospective ones for long wavelength THz generation by phase-matched parametric processes. It demonstrates evident advantages in comparison with widely used MgO-doped  $\text{LiNbO}_3$  crystals. Available growth technology for producing large-size KTP crystals and TW-level pump systems can allow generation of high-power ps-scale THz pulses.

**Author Contributions:** Conceptualization, Y.A.; Methodology, A.M. (Arkady Meshalkin) and V.A.; Software, A.M. (Alexander Mamrashev) and G.L.; Formal Analysis, A.M. (Alexander Mamrashev), N.N. and G.L.; Investigation, N.N. and A.M. (Arkady Meshalkin); Data Curation, A.M. (Alexander Mamrashev), N.N., G.L.; Writing-Original Draft Preparation, Y.A.; Writing-Review & Editing, A.M. (Alexander Mamrashev), N.N. and Y.A.; Visualization, G.L.; Supervision, Y.A. and V.A.

**Funding:** This research was funded by Russian Foundation for Basic Research (RFBR) grant number 17-32-80039 and complex program of basic academic research of Russian Ministry of Science and Higher Education (State Registration No. AAAA-A17-117052410033-9).

**Acknowledgments:** The terahertz spectroscopy measurements were carried out on the time-domain terahertz spectrometer at the Shared Equipment Center “Spectroscopy and Optics” of the Institute of Automation and Electrometry SB RAS, Novosibirsk, Russia.

**Conflicts of Interest:** The authors declare no conflict of interest.

## References

1. Nikogosyan, D. *Nonlinear Optical Crystals: A Complete Survey*; Springer: New York, NY, USA, 2005; ISBN 978-0-387-22022-2.
2. Sorokina, N.I.; Voronkova, V.I. Structure and properties of crystals in the potassium titanyl phosphate family: A review. *Crystallogr. Rep.* **2007**, *52*, 80–93. [[CrossRef](#)]
3. Haiyong, Z.; Ge, Z.; Chenghui, H.; Yong, W.; Lingxiong, H.; Zhenqiang, C. Multi-watt power blue light generation by intracavity sum-frequency-mixing in  $\text{KTiOPO}_4$  crystal. *Opt. Express* **2008**, *16*, 2989–2994. [[CrossRef](#)] [[PubMed](#)]
4. Bhar, G.C.; Rudra, A.M.; Chaudhary, A.K.; Sasaki, T.; Mori, Y. Highly efficient difference-frequency generation in KTP. *Appl. Phys. B Laser Opt.* **1996**, *63*, 141–144. [[CrossRef](#)]
5. Bhar, G.C.; Chatterjee, U.; Rudra, A.M.; Chaudhary, A.K. Generation of widely tunable mid-infrared radiation by difference frequency mixing in KTP. *J. Phys. D Appl. Phys.* **1997**, *30*, 2693–2697. [[CrossRef](#)]
6. Zheng, J.; Zhao, S.; Wang, Q.; Zhang, X.; Chen, L. Influence of thermal effect on KTP type-II phase-matching second-harmonic generation. *Opt. Commun.* **2001**, *199*, 207–214. [[CrossRef](#)]
7. Colville, F.G.; Dunn, M.H.; Ebrahimzadeh, M. Continuous-wave, singly resonant, intracavity parametric oscillator. *Opt. Lett.* **1997**, *22*, 75–77. [[CrossRef](#)] [[PubMed](#)]
8. Isaienko, O.; Borguet, E. Generation of ultra-broadband pulses in the near-IR by non-collinear optical parametric amplification in potassium titanyl phosphate. *Opt. Express* **2008**, *16*, 3949–3954. [[CrossRef](#)] [[PubMed](#)]
9. Tang, M.; Minamide, H.; Wang, Y.; Notake, T.; Ohno, S.; Ito, H. Dual-wavelength single-crystal double-pass KTP optical parametric oscillator and its application in terahertz wave generation. *Opt. Lett.* **2010**, *35*, 1698–1700. [[CrossRef](#)] [[PubMed](#)]
10. Wang, W.; Cong, Z.; Chen, X.; Zhang, X.; Qin, Z.; Tang, G.; Li, N.; Wang, C.; Lu, Q. Terahertz parametric oscillator based on  $\text{KTiOPO}_4$  crystal. *Opt. Lett.* **2014**, *39*, 3706–3709. [[CrossRef](#)] [[PubMed](#)]
11. Wu, M.-H.; Chiu, Y.-C.; Wang, T.-D.; Zhao, G.; Zukauskas, A.; Laurell, F.; Huang, Y.-C. Terahertz parametric generation and amplification from potassium titanyl phosphate in comparison with lithium niobate and lithium tantalate. *Opt. Express* **2016**, *24*, 25964–25973. [[CrossRef](#)] [[PubMed](#)]
12. Rusov, V.A.; Serebryakov, V.A.; Kaplun, A.B.; Gorchakov, A.V. Using modulators based on KTP crystals in Nd: YAG lasers with high mean power. *J. Opt. Technol.* **2009**, *76*, 325–331. [[CrossRef](#)]

13. Rusov, V.A.; Zakharova, N.A.; Kaplun, A.B.; Meshalkin, A.B.; Gorshakov, A.V. Study of the electrical-conductivity kinetics of KTP crystals used in the modulators of solid-state lasers. *J. Opt. Technol.* **2013**, *80*, 532–536. [[CrossRef](#)]
14. Rusov, V.A.; Serebryakov, V.A.; Doroganov, S.V.; Kalintseva, N.A.; Narivonchik, A.S.; Skvortsov, D.V. Electro-optical modulators based on KTP crystals for high-power lasers in the mid-IR region. *J. Opt. Technol.* **2016**, *83*, 716–721. [[CrossRef](#)]
15. Stepanov, A.G.; Henin, S.; Petit, Y.; Bonacina, L.; Kasparian, J.; Wolf, J.-P. Mobile source of high-energy single-cycle terahertz pulses. *Appl. Phys. B* **2010**, *101*, 11–14. [[CrossRef](#)]
16. Wyncke, B.; Brehat, F.; Mangin, J.; Marnier, G.; Ravet, M.F.; Metzger, M. Infrared reflectivity spectrum of KTiOPO<sub>4</sub> single crystal. *Phase Transit.* **1987**, *9*, 179–183. [[CrossRef](#)]
17. Kugel, G.E.; Brehat, F.; Wyncke, B.; Fontana, M.D.; Marnier, G.; Carabatos-Nedelec, C.; Mangin, J. The vibrational spectrum of a KTiOPO<sub>4</sub> single crystal studied by Raman and infrared reflectivity spectroscopy. *J. Phys. C Solid State Phys.* **1988**, *21*, 5565. [[CrossRef](#)]
18. Mounaix, P.; Sarger, L.; Caumes, J.P.; Freysz, E. Characterization of non-linear potassium crystals in the terahertz frequency domain. *Opt. Commun.* **2004**, *242*, 631–639. [[CrossRef](#)]
19. Sang, M.; Fan, L.; Lu, X.; Zhang, W. Optical phonon resonance of KTiOPO<sub>4</sub> crystal characterized by THz time-domain spectroscopy. *Acta Photonica Sin.* **2009**, *32*, 1286–1290.
20. Antsygin, V.D.; Kaplun, A.B.; Mamrashev, A.A.; Nikolaev, N.A.; Potaturkin, O.I. Terahertz optical properties of potassium titanyl phosphate crystals. *Opt. Express* **2014**, *22*, 25436–25443. [[CrossRef](#)] [[PubMed](#)]
21. Huang, J.-G.; Huang, Z.-M.; Nikolaev, N.A.; Mamrashev, A.A.; Antsygin, V.D.; Potaturkin, O.I.; Meshalkin, A.B.; Kaplun, A.B.; Lanskii, G.V.; Andreev, Y.M.; et al. Phase matching in RT KTP crystal for down-conversion into the THz range. *Laser Phys. Lett.* **2018**, *15*, 075401. [[CrossRef](#)]
22. Yeh, K.-L.; Hoffmann, M.C.; Hebling, J.; Nelson, K.A. Generation of 10 μJ ultrashort terahertz pulses by optical rectification. *Appl. Phys. Lett.* **2007**, *90*, 171121. [[CrossRef](#)]
23. Unferdorben, M.; Szaller, Z.; Hajdara, I.; Hebling, J.; Pálfalvi, L. Measurement of refractive index and absorption coefficient of congruent and stoichiometric lithium niobate in the terahertz range. *J. Infrared Millim. Terahertz Waves* **2015**, *36*, 1203–1209. [[CrossRef](#)]
24. Alekseev, S.V.; Ivanov, M.V.; Ivanov, N.G.; Losev, V.F.; Mesyats, G.A.; Panchenko, Y.N.; Ratakhin, N.A. Parameters of the THL-100 hybrid femtosecond laser system after modernization. *Russ. Phys. J.* **2015**, *58*, 1087–1092. [[CrossRef](#)]



© 2018 by the authors. Licensee MDPI, Basel, Switzerland. This article is an open access article distributed under the terms and conditions of the Creative Commons Attribution (CC BY) license (<http://creativecommons.org/licenses/by/4.0/>).